Supplemental Data

Heparin-dependent amyloid fibrillation of hen egg white lysozyme reveals distinct mechanisms of fibrillation

Ayame Nitani, Hiroya Muta, Masayuki Adachi, Masatomo So, Kenji Sasahara, Kazumasa Sakurai, Eri Chatani, Kazumitsu Naoe, Hirotsugu Ogi, Damien Hall, and Yuji Goto

SI Methods

Gold nanoparticles coated with sulfate groups. Preparation of gold nanoparticles with sulfate groups was achieved by mixing two solutions of reverse micelles, one containing the Au salt and the other a mixture of reducing agent and stabilizing agent. Hydrazine (N_2H_4) was selected as the reducing agent. In a typical experiment, 36 μL of 0.75 M aqueous hydrazine solution containing 0.144 μmol sodium 3-mercapto-1-propanesulfonate (MPS) was added to 4.98 mL of 0.10 M bis(2-ethylhexyl)sulfosuccinate sodium (AOT) in isooctane. An equal volume of reverse micelles with 45 μL of 0.20 M gold (III) chloride ($HAuCl_4$) solution was also prepared. Immediately after vigorous mixing of the two reverse micelle solutions, the solution was allowed to settle for 2 h. After settling, 20 mL of ethanol was added, with this step followed by addition of 10 mL of acetone. The red precipitate was recovered after centrifugation at 3000 rpm for 20 min, and re-dispersed in 5.0 mL of acetone by ultrasonication for 1 min. The precipitate was recovered after centrifugation at 3,000 rpm for 10 min. The washing step with acetone was repeated three times. Finally the collected precipitate was re-dispersed in 4 mL of water. From TEM measurement the average diameter of the metal core of the Au nanoparticles was 5.6 nm with a total variation in size distribution of 4.8%.

Dynamic Light Scattering (DLS) Measurements. DLS measurements were performed with a Zetasizer Nano-S equipped with a He-Ne laser of 633 nm wavelength (Malvern Instruments Ltd., Worcestershire, UK). A 2 mg/mL solution of HEWL was prepared in 10 mM HCl containing 100 mM NaCl and concentrations of heparin ranging from 0 to 37.5 mg/mL. The samples were then incubated at 25 or 60 °C with or without agitation. An Eppendorf ThermoMixer C (Eppendorf, Hamburg, Germany) set at 60 °C and 1,200 rpm was used to provide agitation. After a 1-day incubation, the samples were transferred into a quartz cell and the dynamic light scattering was monitored. The temperature of the sample was kept constant throughout the measurement. From the time-dependent fluctuation of the light scattering intensity, an autocorrelation function was generated. For all measurements, the autocorrelation function was fitted to an equation, $g^{(2)}(\tau) - 1$, based on a sum of exponential terms,

$$g^{(2)}(\tau) - 1 = \beta\left(\sum_{i=1}^{n} A_i e^{-D_i q^2 \tau}\right)^2 \qquad \text{(S1)}.$$

Here, n is the number of components, A_i is amplitude of the i^{th} component, D_i is diffusion constant of the i^{th} component, q is scattering vector, and β is a constant. The scattering vector q was defined as $q = 4\pi n_0 \sin(\theta/2)/\lambda_0$, with n_0 being the refractive index of the solvent, θ the scattering angle measured from the forward direction and λ_0 the wavelength of the laser. θ and λ_0 were assigned respective values of 173° and 633 nm based on the manufacturer's specifications. The solvent refractive index, n_0, for a 10 mM HCl solution containing 100 mM NaCl was calculated to be 1.331 at both 25 °C and 60 °C using Dispersion Technology Software 5.00 (Malvern Instruments Ltd.). For the samples containing heparin, the contribution

of heparin to the solvent refractive index was estimated using a specific refractive increment for heparin of dn_0/dc = 0.131 mL/g (1). From the measured D_i values, hydrodynamic radii of the ith component (R_{hi}) were estimated using the following equation,

$$R_{hi} = \frac{k_B T}{6\pi\eta D_i} \qquad \text{(S2)},$$

where k_B is Boltzmann's constant, T is the measurement temperature (298 or 333 K), and η is the solvent viscosity. The value of η for a 10 mM HCl solution containing 100 mM NaCl was calculated as 8.951×10^{-4} Pa·s at 25 °C or 4.792×10^{-4} Pa·s at 60 °C. The contributions of various concentrations of heparin to the solvent viscosity were determined using an empirical relation based on the intrinsic viscosity of heparin (2). The volume fraction of each component particle was estimated from the value A_i (see Eqn. S1), which relates to the relative amplitude of scattered light intensity of the i^{th} component. Under the assumption that this value is proportional to the sixth power of the particle radius, the component volume fraction can be estimated by dividing A_i by the cube of R_{hi}.

Analytical Ultracentrifuge Analysis. The molecular weight, absorbance extinction coefficient, and partial specific volume ($\bar{v}$) of HEWL were calculated from its amino acid sequence to be 14,300 g mole^{-1}, 2.69 mL mg^{-1} cm^{-1} at 280 nm, and 0.729 mL g^{-1}, respectively (3,4). The viscosity (η) of the standard buffer for the present ultracentrifuge measurement, 10 mM HCl and 100 mM NaCl at 25 °C, was estimated approximately to be 8.951×10^{-4} Pa·s as described above. The contributions of various concentrations of heparin to the solvent viscosity were also estimated as described above (2). The solvent density (ρ_0) was directly determined by weighing 1 mL of buffer.

HEWL was dissolved in the standard buffer (10 mM HCl (pH ~2.0), 100 mM NaCl) containing various concentration of heparin. The concentration of HEWL was 0.25 mg/ml, giving an absorbance of 0.67 at 280 nm. The sample solutions were placed in assembled cells with sapphire windows and 12-mm path length aluminum centerpieces. The cells were set in a four-holed Beckman–Coulter An60-Ti rotor. Both the sedimentation velocity and equilibrium data were collected using the absorption detection system of an XL-I analytical ultracentrifuge (Beckman–Coulter).

Before the sedimentation velocity experiments, the rotor with cells was allowed to attain temperature equilibrium at 25 °C for 1 h under vacuum. Samples were first centrifuged at 3,000 rpm for detection of large aggregate. If species that sediment at 3,000 rpm were detected, radial scans were repeated until the absorbance profile becomes flat. After that, the rotor speed was increased to 60,000 rpm and radial scans were further repeated. All radial scans were carried out at 280 nm at intervals of 5–7 min with a radial increment of 0.001 cm in the continuous scanning mode under a constant temperature of 25 °C. It is noted that no species that preferably sediments at 3,000-60,000 rpm was detected in the preliminary measurement.

The obtained data were analyzed using Sedfit (version 15.52) (5,6). The *c*(*M*) continuous distribution model was selected. An initial *c*(*M*) distribution was generated with initial estimates of fitting parameters, *i.e.*, radial position for the cell bottom, an initial position for meniscus, radial data range, and frictional coefficient ratio (f/f_0), and basic information for fitting, *i.e.*, molecular weight range, $\bar{v}$ of HEWL, solvent viscosity (η) and density (ρ). Then the *c*(*M*) distribution was optimized using the meniscus position and *baseline* as floating parameters with a fixed f/f_0 value of 1.2. Time-independent noise correction was not used during data analysis.

Sedimentation equilibrium measurements were conducted at 25,000 and 32,000 rpm at 25 °C. Absorbance (*A*)-versus-radius (*r*) data were acquired as an average of 20 absorbance measurements at 280 nm over 0.001-cm intervals. For the samples containing 0 or 2.5 μg/mL heparin, the data were obtained after 20 h of centrifugation. On the other hand, for the sample containing 37.5 mg/mL heparin, the *A* vs *r* data profile was found to change gradually. Thus, the *A* vs *r* data profiles were recorded after 23, 89, and 141 h after of centrifugation. The *A* vs *r* data were fitted to the following equation assuming a single size component with a molecular weight M_w:

$$A(r) = A(r_0)\exp[(\omega^2/2RT)M_w(1-\bar{v}\rho_0)(r^2-r_0^2)] + A_0 \qquad \text{(S3)},$$

where r_0 is the reference radius point, ω is angular velocity, A_0 is baseline absorbance, R is the gas constant, and T is temperature in Kelvin (5). Nonlinear least-squares fitting was performed with Igor Pro software.

Supplemental Results

Isothermal titration calorimetry (ITC) to examine the heparin-HEWL interactions. To examine the affinity of negatively charged heparin and positively charged HEWL, we performed a series of ITC measurements in 10 mM HCl (pH 2.0) using a PEAQ-ITC instrument (Malvern Instruments, UK) (supplemental Fig. S2). Titration of 0.01 mg/ml heparin in the ITC cell at 37 °C by 3 μl each of 1 mg/ml HEWL in the syringe showed a saturating titration reaction (supplemental Fig. S2B). The stoichiometry of binding was one heparin interacting with 3.8 mol of HEWL with a dissociation constant, K_D, of 5. 6 nM for each binding site, revealing an exothermic strong binding. The free energy change and enthalpy change of binding were -11.7 and -13.4 kcal/mol, respectively. Heparin with an average molecular weight of 13,000 contains 24-70 negative charges depending on 1-3 sulfate groups per disaccharide unit. In contrast, HEWL with a molecular weight of 14,300 has a net charge of +19 at pH 2. The similar strong interaction was obtained at 0.025 mg/ml of heparin (supplemental Fig. S2C).

On the other hand, at heparin concentrations between 0.1 – 10 mg/ml, the titration reaction did not saturate because of the shortage of HEWL (supplemental Fig. S2D-F). The exothermic heat effect observed

for each injection of HEWL was independent of heparin concentration, suggesting that the initial affinity was independent of heparin concentration. At 100 mg/ml heparin, the apparent exothermic heat was less than those at lower heparin concentrations, suggesting a different mechanism of fibril formation (supplemental Fig. S2G). However, a larger heat effect caused by the dilution of heparin at higher heparin concentrations precluded the exact interpretation.

Low-Temperature Trapping and High Temperature-induced Fibrillation. CD spectra recorded at 25 °C following addition of various concentrations of heparin, indicated that aggregates containing HEWL exhibited native HEWL structure at either low or high heparin concentrations (Fig. 3B, supplemental Fig. S1). To characterize the size of oligomeric native aggregates at both very low and high concentrations of heparin, we performed DLS measurements on solutions containing various concentrations of heparin, previously subjected to overnight incubation at 25 or 60 °C, or at 60 °C under agitation (supplemental Fig. S5, supplemental Table S1). Results did not depend significantly on the period of incubation (i.e., 1 h, 3 h, or overnight). We report our findings in terms of the R_h (hydrodynamic radius) of the dominant species constituting more than 90% of the calculated volume fraction.

In the absence of heparin at 25 °C, R_h was 2.2 nm, consistent with monomeric native HEWL (R_h = 3.2 nm (7)). Upon addition of 2.5 μg/mL heparin, R_h increased to 6.9 nm. Increases in the concentration of heparin up to 0.2 mg/ml increased the major component hydrodynamic radius to 536 nm. Further increase in heparin concentration decreased R_h to 112.7 nm at 20 mg/mL. Incubation of the HEWL solutions at 60 °C increased the R_h values at all heparin concentrations. However, incubation at 60 °C with agitation by shaking decreased the R_h values at low (2.5 and 20 μg/ml) and high (37.5 mg/ml) heparin concentrations, suggesting a role for ultrasonication-dependent dispersion of aggregates. Under these conditions, we detected no fibrillation.

Native oligomers in the presence of heparin were also characterized by analytical ultracentrifugation at 25 °C (supplemental Fig. S6, Table S1). Sedimentation velocity measurements were performed with 0.25 mg/ml HEWL at 0, 2.5, and 10 μg/mL, and 22.5 mg/mL heparin and 25 °C. The molecular weights of major species were 18000, 20000, 19000, and 40000 at 0, 2.5, and 10 μg/mL, and 22.5 mg/mL heparin, respectively. The results indicated that, although oligomers were dominant at 22.5 mg/mL heparin, monomers were dominant at low heparin concentrations. Sedimentation equilibrium measurements at 0, 2.5, and 37.5 mg/mL heparin estimated the apparent molecular weight to be 15200, 14300, and 18200 g $mole^{-1}$, respectively, suggesting that the extents of aggregation were low even at 37.5 mg/mL. Although this result differs somewhat from the dynamic light scattering measurements, the discrepancy may be due to the fact that any very large aggregates may be effectively pelleted out at the speed regime used in the AUC experiments.

Taken together, both DLS and analytical ultracentrifugation measurements indicate that, although a small amount of hetero-oligomeric HEWL (native state) existed at 25 °C, at low and high heparin concentrations, the extents of aggregation were not high. At 60 °C where HEWL was denatured, the size of amorphous aggregates at 0.02 – 10 mg/mL heparin monitored by DLS increased significantly. However, in the presence of 37 mg/mL heparin, the size of oligomers decreased, probably due to stabilization of the native state (supplemental Fig. S5).

Fibrillation in 50% (v/v) TFE in the Presence of Salts and Heparin. We previously reported amyloid formation from HEWL solutions containing trifluoroethanol (TFE) at pH 4.7 with applied ultrasonication (8). To further clarify the effects of heparin, we examined both heparin and simple salt-induced fibrillation of HEWL in 50% (v/v) TFE at 37 °C under ultrasonication (supplemental Fig. S9). In the absence of salt, the lag time was both long (> 6 h) and highly variable (supplemental Fig. S9A). Low concentrations of added heparin (< 5 μg/mL) accelerated fibrillation (as shown by a decrease in lag time) and increased the maximal ThT fluorescence in a concentration dependent manner. At heparin concentrations above 10 μg/mL, the final fluorescence intensity decreased sharply, with this decrease accompanied by an increase in the total light scattering. Above 10 μg/mL heparin, extensive aggregation was observed. As the solubility limit of heparin in 50% TFE was ~1 mg/ml, the effect of higher heparin concentrations could not be examined under these conditions.

The effects of NaCl (supplemental Fig. S9D-F) and Na_2SO_4 (supplemental Fig. S9G-I) in 50% TFE were also examined; both salts accelerated fibrillation at low concentrations with optima at 0.1 and 0.01 M, respectively (in terms of recorded effects on ThT intensity and lag time). However the effect of NaCl concentrations above 0.4 M or Na_2SO_4 concentrations above 0.1 M could not be examined due to salt-induced TFE/aqueous phase separation. The extent of enhancement by heparin, NaCl and Na_2SO_4 on the fibrillation of HEWL in 50% TFE exhibited the following positional ordering: heparin >> Na_2SO_4 > NaCl. This finding was consistent with that obtained in 10 mM HCl. Results also showed that a V-shaped dependence of lag time on the additive concentration operates in 50% TFE.

Au Nanoparticle-Dependent Fibrillation in 50% TFE. To further investigate the role of electrostatic attractions between negatively charged heparin and positively charged HEWL, we used gold nanoparticles coated with sulfate groups (supplemental Fig. S10E). We adopted the conditions of 50% (v/v) TFE at pH 4.7 and 37 °C, due to the fact that gold nanoparticles underwent time dependent aggregation in 10 mM HCl. Analysis by fluorometric recording under a continuous cyclical regimen (involving 1 min-ultrasonication followed by 9 min-quiescence) revealed a lag time of approximately 9 h (supplemental Fig. S10A). For gold nanoparticle concentrations between 0.5 and 50 nM, fibrillation lag times were reduced upon increasing the concentration of nanoparticle (supplemental Fig. S10B-D, F). No change in final ThT fluorescence and light

scattering intensity accompanied the observed enhancement of rate (supplemental Fig. S10G, H). When HANABI was used, a similar gold nanoparticle concentration-dependent acceleration was observed (supplemental Fig. S10I-N). The CD spectra confirmed that, although HEWL in 50% (v/v) TFE at pH 4.7 assumed an α-helical conformation, it transformed to fibrils upon ultrasonic treatment (supplemental Fig. S10O, P). TEM images (supplemental Fig. S10Q-U) showed fibrillar morphologies in which mixtures of fibrils and nanoparticles were observed at high nanoparticle concentrations (e.g. 50 nM). These results further confirmed that multivalent anions effectively trigger fibrillation of HEWL by forming protein-Au nanoparticle complexes stabilized by charge-charge attractions. We recognize that, in the case of Au nanoparticle-induced acceleration, an increase in ThT fluorescence was not preceded by an increase in light scattering (supplemental Fig. S10B-D), indicating that HEWL adsorption to the gold nanoparticle surface did not induce multiple-nanoparticle complexes even if the heterogeneous nucleation event takes place on the surface of the nanoparticle.

Supplemental References

1. Sommers, C. D., Ye, H., Kolinski, R. E., Nasr, M., Buhse, L. F., Al-Hakim, A., and Keire, D. A. (2011) Characterization of currently marketed heparin products: analysis of molecular weight and heparinase-I digest patterns. *Anal Bioanal Chem* **401**, 2445-2454
2. Chung, M. C., and Ellerton, N. F. (1976) Viscosity at low shear and circular dichroism studies of heparin. *Biopolymers* **15**, 1409-1423
3. Gill, S. C., and von Hippel, P. H. (1989) Calculation of protein extinction coefficients from amino acid sequence data. *Anal Biochem* **182**, 319-326
4. Harpaz, Y., Gerstein, M., and Chothia, C. (1994) Volume changes on protein folding. *Structure* **2**, 641-649
5. Lebowitz, J., Lewis, M. S., and Schuck, P. (2002) Modern analytical ultracentrifugation in protein science: a tutorial review. *Protein Sci* **11**, 2067-2079
6. Dam, J., and Schuck, P. (2004) Calculating sedimentation coefficient distributions by direct modeling of sedimentation velocity concentration profiles. *Methods Enzymol* **384**, 185-212
7. Yamazaki, T., Kimura, Y., Vekilov, P. G., Furukawa, E., Shirai, M., Matsumoto, H., Van Driessche, A. E., and Tsukamoto, K. (2017) Two types of amorphous protein particles facilitate crystal nucleation. *Proc Natl Acad Sci U S A* **114**, 2154-2159
8. Lin, Y., Lee, Y. H., Yoshimura, Y., Yagi, H., and Goto, Y. (2014) Solubility and supersaturation-dependent protein misfolding revealed by ultrasonication. *Langmuir* **30**, 1845-1854

Table S1. DLS and analytical ultracentrifuge analyses of oligomeric states of HEWL in the presence of heparin.

heparin	0 mg/mL	2.5 μg/mL	10 (AUC) or 20 (DLS) μg/mL	0.2 mg/ml	2 mg/ml	20 (DLS) or 22.5 (AUC) mg/mL	37.5 mg/mL
DLS, 25°C (quiescence)	2.2±0.2 (1.00)	6.9±3.9 (1.00)	306.7±237.7 (0.98) 2571.8±446.5 (0.02)	536.4±77.3 (0.97) 3760.6±96.6 (0.03)	190.0±52.7 (0.97) 1408.4±368.4 (0.03)	112.7±77.9 (0.97) 608.3±149.2 (0.03)	0.5±0.0 (1.00)
DLS, 60°C(quiescence)	26.9±2.1(0.99) 200.5±7.0 (0.01)	110.6±42.1 (1.00)	1718.4±120.4 (1.00)	1999.0±246.1 (1.00)	1125.9±172.0 (1.00)	2281.7±92.6 (1.00)	1240.4±241.0 (1.00)
DLS, 60°C(agitation)	28.3±1.5 (0.99) 170.6±11.6 (0.01)	50.6±3.8 (1.00)	12.7±3.1 (1.00)	2469.3±1971.4 (1.00)	3319.4±1207.9 (1.00)	3617.4±235.1 (1.00)	0.5±0.0 (1.00)
AUC results	SE: 15236 Da, single species SV: 14940±1451 Da (dominant) 48077±4653 Da (minor, 0.38% of dominant species)	SE: 14333 Da, single species SV: 15796±2235 Da (dominant)	SV: large species (rapidly sedimenting at 3000 rpm) 15965±1867 Da (dominant) 49817±4901 Da (minor, 2.84% of dominant species)			SV: large species (gradually sedimenting at 3000 rpm) 33431±2792 Da (dominant)	SE: single species, time-dependent Mw 18174 (23 h) 19675 (89 h) 20458 (141h)

Fig. S1. Thermal unfolding of HEWL in the presence of various concentrations of heparin. (A, C, E, G, I, K, M, and O) Thermal unfolding was monitored by ellipticity at 220 nm at various concentrations of heparin as indicated. Transition curves were fitted assuming a two-state mechanism. The midpoint temperature is shown for each transition. (B, D, F, H, J, L, M, and P) CD spectra before and after the thermal unfolding. (Q) Dependence of midpoint temperature against heparin concentration. Heparin concentrations between 0.5-10 mg/mL were not examined because of significant aggregation.

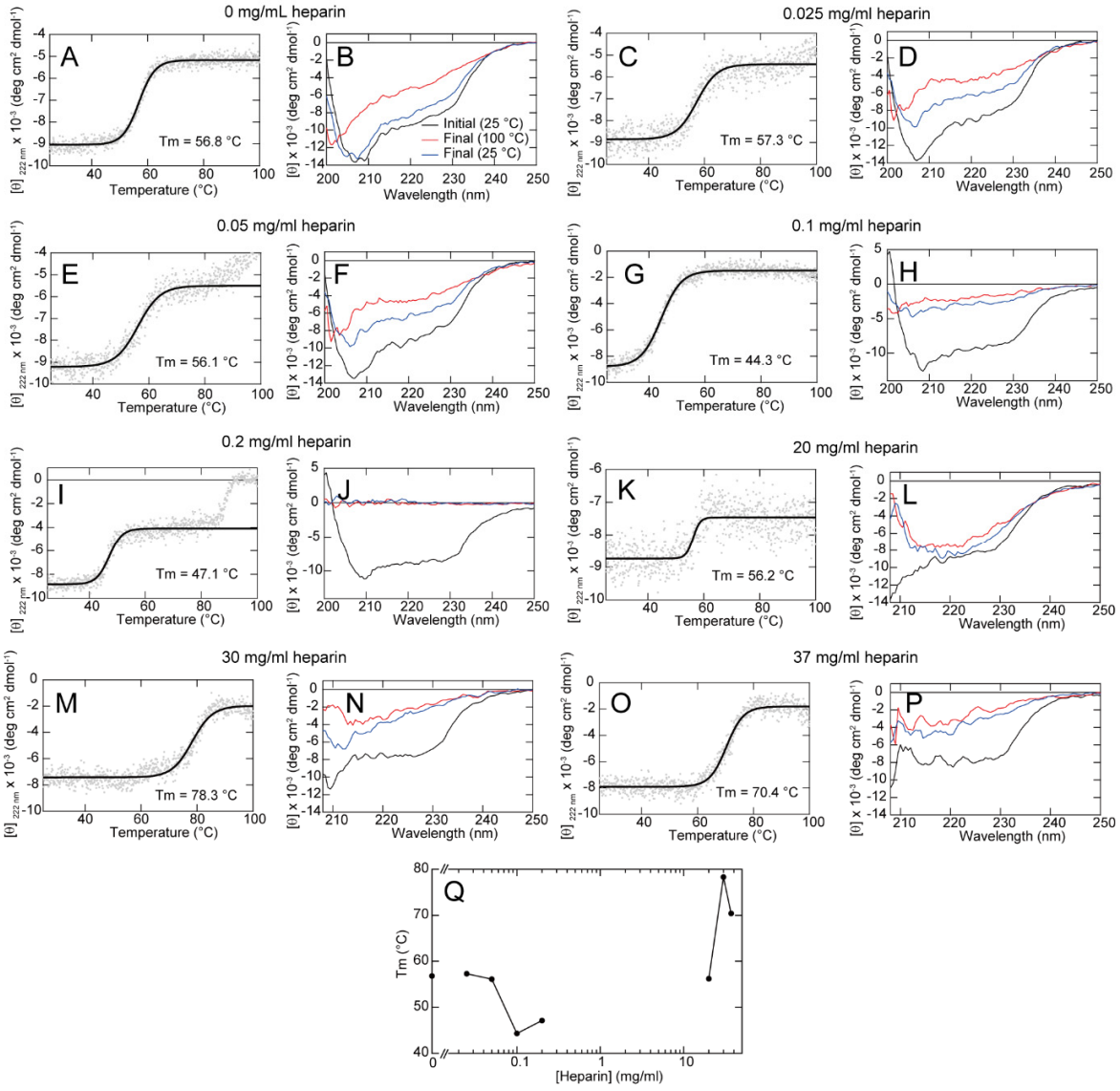

Fig. S2. ITC measurements to examine the heparin-HEWL interactions. Heparin concentrations were 0 (A), 0.01 (B), 0.025 (C), 0.1 (D), 1 (E), 10 (F), and 100 (G) mg/ml. Upper, middle, and lower panels show the direct heat effects for the injection of HEWL, heat effects for the buffer injection, and total heat effects (ΔH) for each injection, respectively. The measurements were done in 10 mM HCl (pH 2.0) at 37 °C using a PEAQ-ITC instrument (Malvern Instruments, UK). A 250 µl of heparin solution in the ITC cell was titrated by 3 µl each of 1 mg/ml HEWL in the syringe.

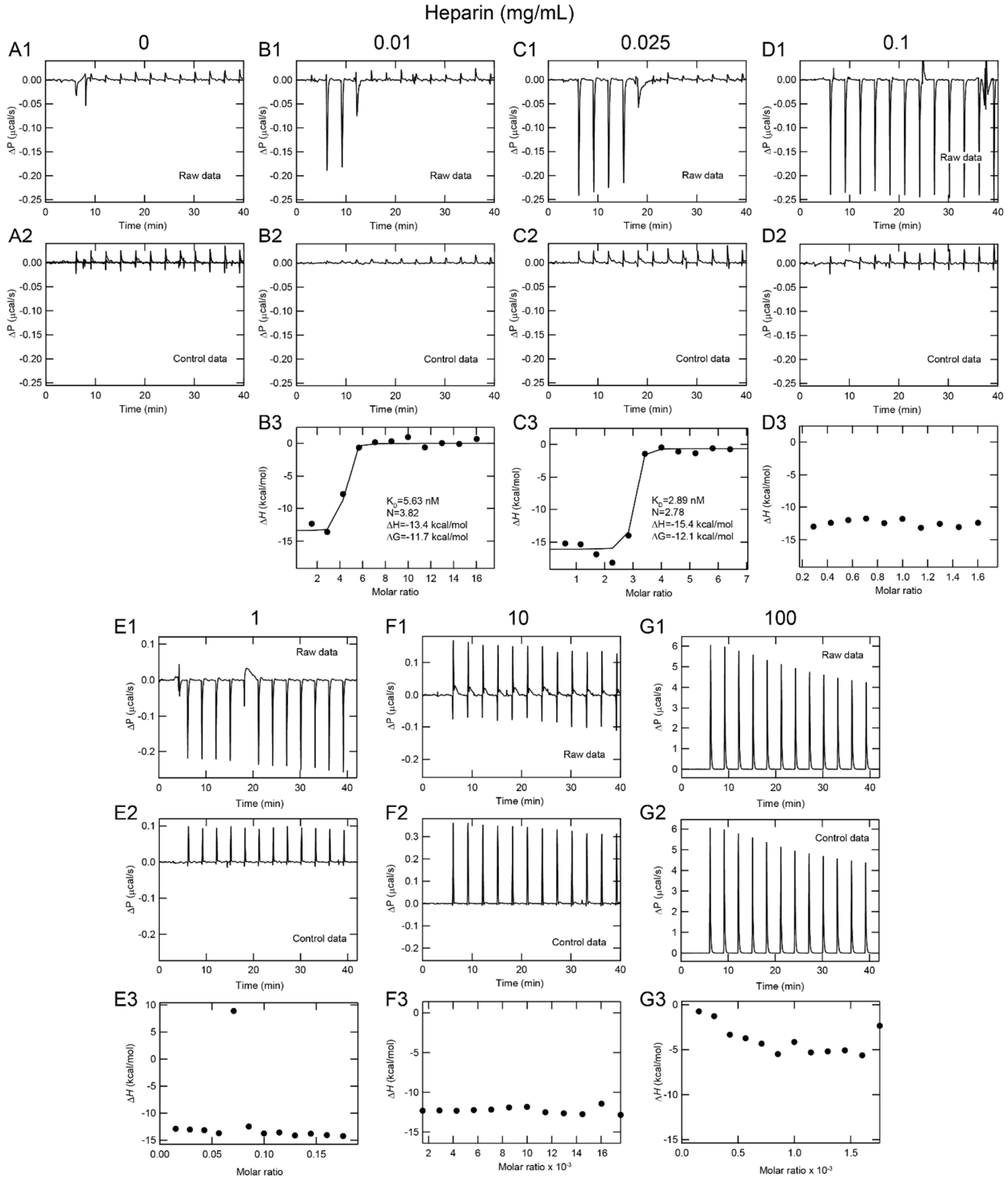

Fig. S3. Distinguishing amorphous aggregates and amyloid fibrils by direct imaging under illumination of white light (A) or ThT fluorography under LED 440 nm light (B). All the solutions contained 5 μM ThT and 10 mM HCl (pH 2.0). Ultrasonicated samples at 60 °C were taken after the measurements with a fluorometer as shown in Fig. 2 and those without ultrasonication were incubated overnight at 60 °C. **(**Row A and B) Dependence on heparin concentration at 0.1 M NaCl after overnight incubation at 60 °C (Row A) or sonication at 60°C (Row B). Concentrations of heparin were the same as those shown in Fig. 4. (Rows C and D) Dependence on NaCl concentration after overnight incubation at 60 °C (Row C) or sonication at 60 °C (Row D). Concentrations of NaCl were the same as those shown in Fig. 4. (Rows E and F) Dependence on Gdn-HCl concentration after overnight incubation at 60°C (Row E) or sonication at 60 °C (Row F). Concentrations of Gdn-HCl were 0 (1), 0.025 (2), 0.05 (3), 0.1 (4), 0.2 (5), 0.4 (6), 0.8 (7), 1.5 (8), 3.0 (9), 4.0 (10), and 6.0 (11) M. (Rows G to H) Dependence on Na_2SO_4 concentration after overnight incubation at 60 °C (Row G) or sonication at 60 °C (Row H). Concentrations of Na_2SO_4 were 0 (1), 0.0025 (2), 0.005 (3), 0.01 (4), 0.025 (5), 0.05 (6), 0.1 (7), 0.2 (8), 0.5 (9), 0.6 (10) and 0.75 (11).

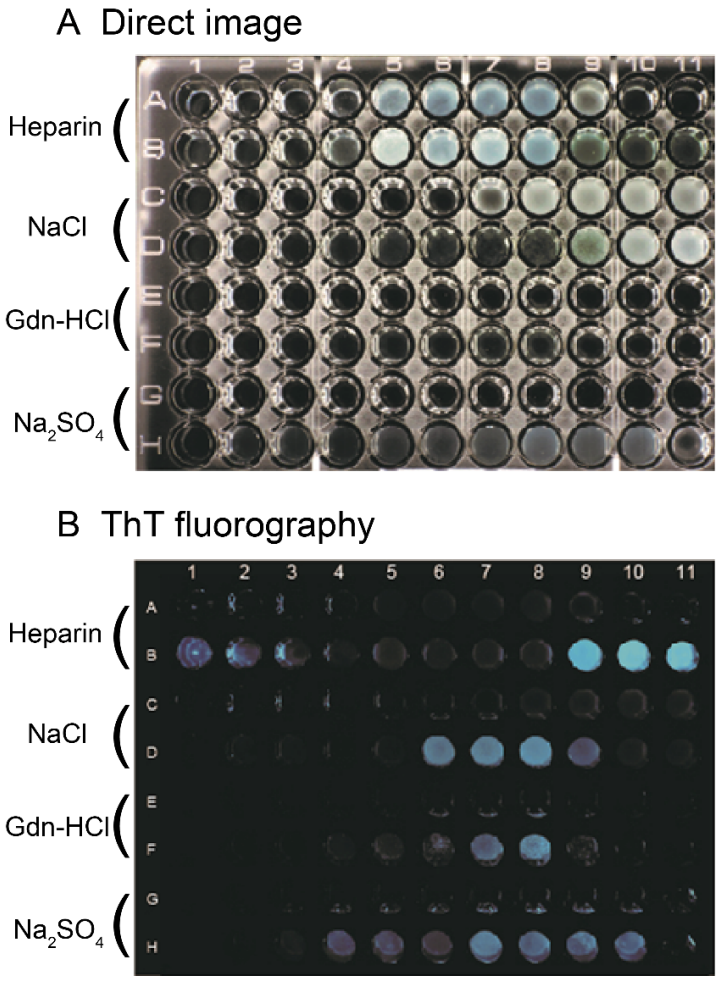

Fig. S4. Low temperature trapping and seeded fibrillation. (A-D) Kinetic trapping at 5 °C and release at 60 °C in 5 (A, B), 19 (C) or 38 (D) mg/mL heparin. Jumps of temperature are indicated by arrows. We note that stabilization of the native state coupled with oligomer formation was responsible for the low-temperature trapping. (E-H) Spontaneous (E, G) and seed-dependent (F, H) fibrillations in the absence (E, F) and presence of 19 mg/mL heparin (G, H). Reactions were monitored by ThT fluorescence at 485 nm (left axis) or light scattering at 445 nm (right axis).

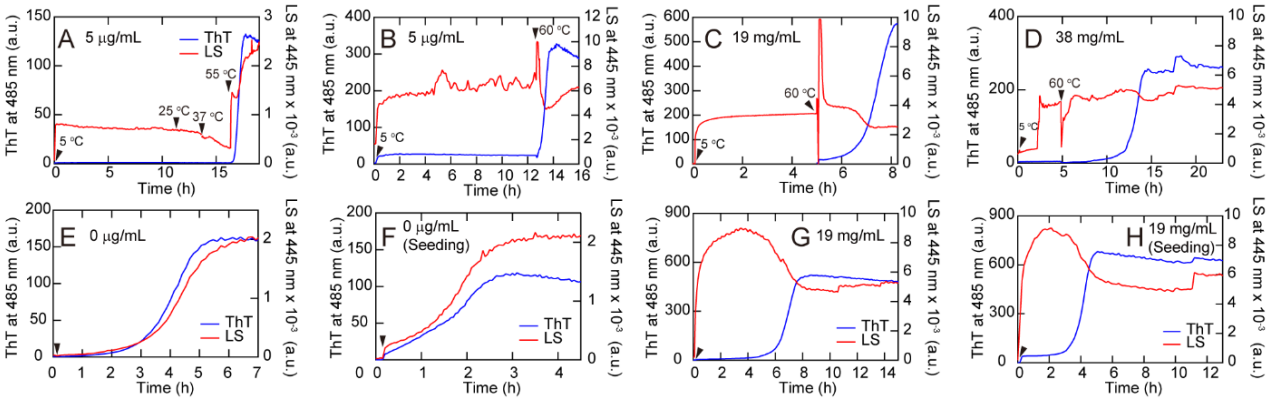

Fig. S5. Conformation of oligomers monitored by dynamic light scattering. (A-C) Plots of autocorrelation functions ($g^{(2)}(\tau)$-1) of scattered light intensity of HEWL solutions. The results of samples incubated at 25 °C under quiescent conditions (A), at 60 °C under quiescent conditions (B), and at 60 °C under agitation (C) are shown. For all incubation conditions, 7 different samples in the absence (0 mg/mL, red) or in the presence of heparin at concentrations of 0.0025 (orange), 0.02 (blue), 0.2 (light green), 2 (green), 20 (magenta), and 37.5 mg/mL (purple) were analyzed. Circles and solid lines represent experimental data and fitted curves, respectively. (D, E) Dependencies of the size of aggregates on heparin concentration. The R_h of the dominant components formed after the one-day incubation at 25 °C under quiescence (black), at 60 °C under quiescence (blue), and at 60 °C under agitation (red) are shown in panel D. A magnified plot of the samples incubated at 25 °C under quiescence is also shown in panel E. The R_h values of the most dominant aggregation components along with other minor components showing volume fractions larger than 1% are summarized in Table S1.

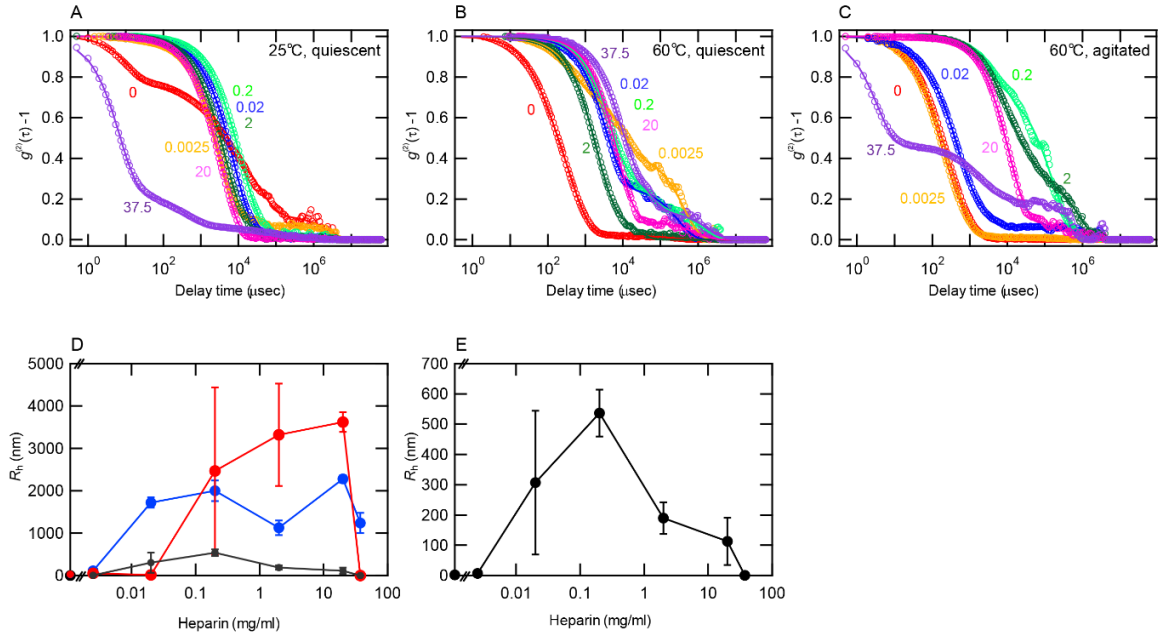

Fig. S6. Conformation of oligomers monitored by analytical ultracentrifuge. (A-D) Raw data of sedimentation velocity measurement at 0 μg/mL (A), 2.5 μg/mL (B), 10 μg/mL (C), and 22.5 mg/mL (D) heparin are shown. The broken lines indicate the initial absorbance for each sample. The blue lines are the scan data obtained at 3,000 rpm. At 0 μg/mL (A) and 2.5 μg/mL (B), the first scan data at 3,000 rpm matched with the broken lines, indicating there were no species sedimenting at 3,000 rpm. At 10 μg/mL heparin (C), the first scan data at 3,000 rpm were flat but lower than the broken lines, indicating the sample contains species that immediately sediments at 3,000 rpm. At 22.5 mg/mL heparin (D), the *A* vs *r* profiles obtained at 3,000 rpm showed a gradual decrease, indicating there were species that gradually sediment at 3,000 rpm. The red and black lines are the data obtained at 60,000 rpm and fitted lines generated by Sedfit, respectively. (E, F) c(*M*) distributions determined by the Sedfit analysis. Panel F shows the same distribution of panel E with an 150-fold expanded y scale. (G-I) Raw data of sedimentation equilibrium measurement at 0 μg/mL (G), 2.5 μg/mL (H), and 37.5 mg/mL (I) heparin. In panels G and H, the *A* vs *r* data obtained at 25,000 rpm and 32,000 rpm are indicated by triangles and circles, respectively. As the *A* vs *r* profiles were gradually changed at 37.5 mg/mL heparin, the time-dependent profiles are shown (I). The red lines are theoretical curves based on Eq. S3.

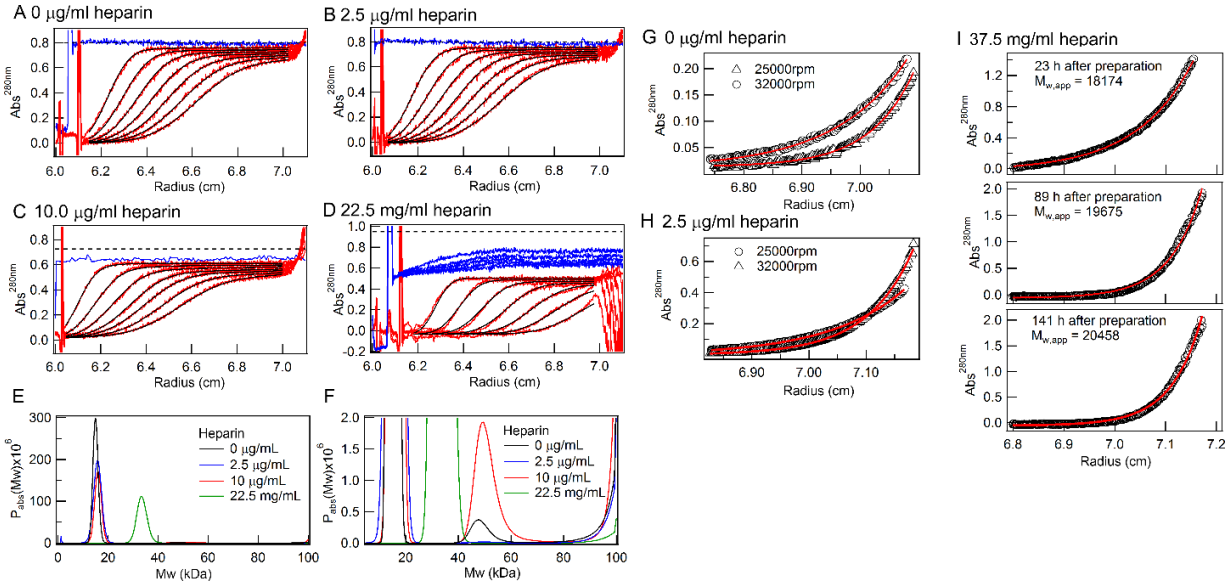

Fig. S7. Fibrillation of HEWL monitored with HANABI at 37 °C. (A, C-K) Kinetics at various heparin concentration monitored by ThT fluorescence. Fibrillation was performed at 0.2 mg/mL HEWL, 0.5 M Gdn-HCl, 10 mM HCl (pH 2.0) and 5 μM ThT. Heparin concentrations were varied between 0-125 mg/mL For all the heparin concentrations, 4 different samples were analyzed are shown in (B-J). Panel (A) show all the data. (B) Dependencies on heparin concentration of maximal ThT fluorescence at 485 nm (left axis, blue points) and lag time (right axis, red points). When no fibrillation was observed, the lag time was assumed to be 30 h.

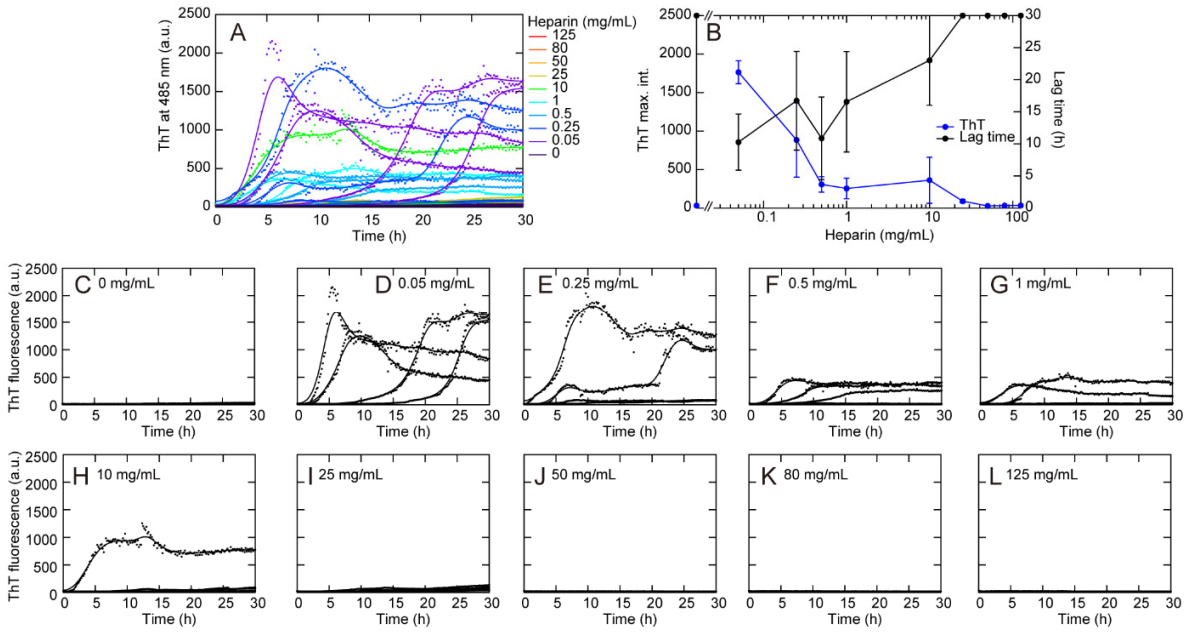

Fig. S8. Fibrillation kinetics at various concentrations of NaCl (A), Gdn-HCl (B), or Na_2SO_4 (C) in 10 mM HCl at 60 °C. Kinetics of HEWL aggregation at various concentrations of salts were monitored for 0.25 mg/ml HEWL under repeated cycles of 4 min ultrasonication and 1 min quiescence under stirring. Kinetics by ThT fluorescence at 485 nm (blue, left axis) and light scattering at 445 nm (red, right axis) were plotted. HEWL was added at 10 min after the start of recording and is indicated by solid arrow head. To confirm the final values, pipette-mixing of the solution was performed at the time point with open arrow head. The increase in the signals indicated the inhomogeneity of the solution because of significant aggregation.

(A) NaCl-dependent fibrillation

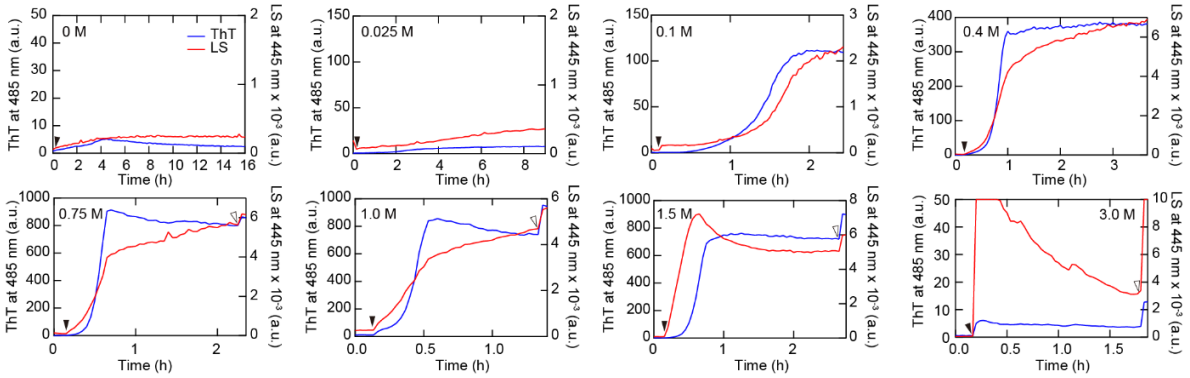

(B) Gdn-HCl-dependent fibrillation

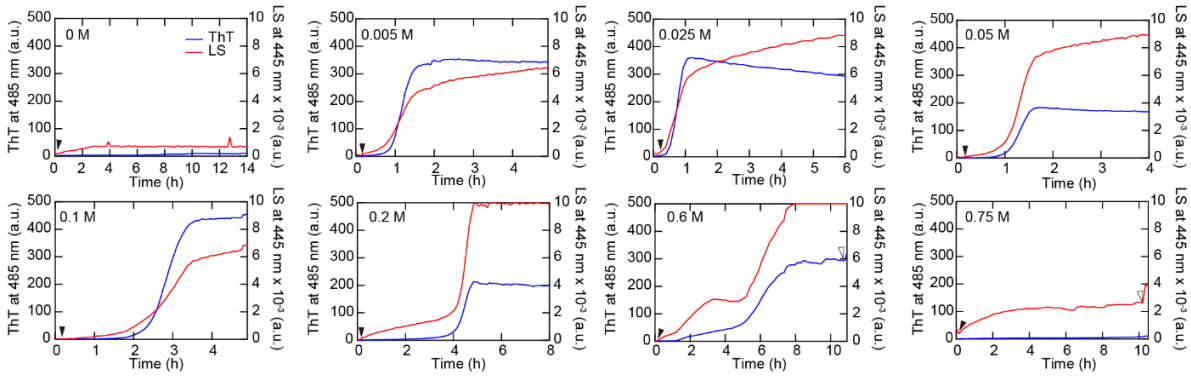

(C) Na_2SO_4-dependent fibrillation

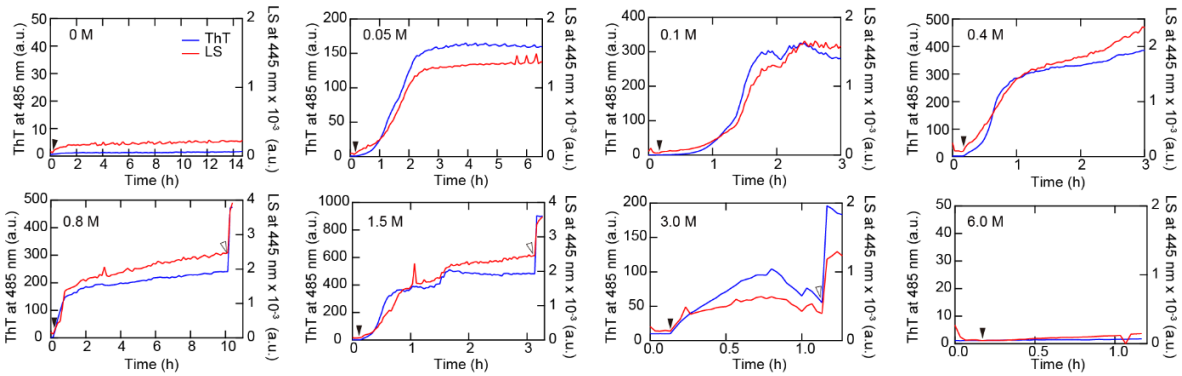

Fig. S9. Effects of heparin (A-C), NaCl (D-F), and Na_2SO_4 (G-I) on fibrillation in 50% (v/v) TFE at pH 4.7 and 37 °C. (A, D, G) Fibrillation kinetics monitored by ThT fluorescence at 485 nm. (B, E, H) Dependencies of ThT fluorescence at 485 nm and light scattering at 445 nm on the salt concentration. (C, F, I) Dependencies of the lag time on the salt concentration.

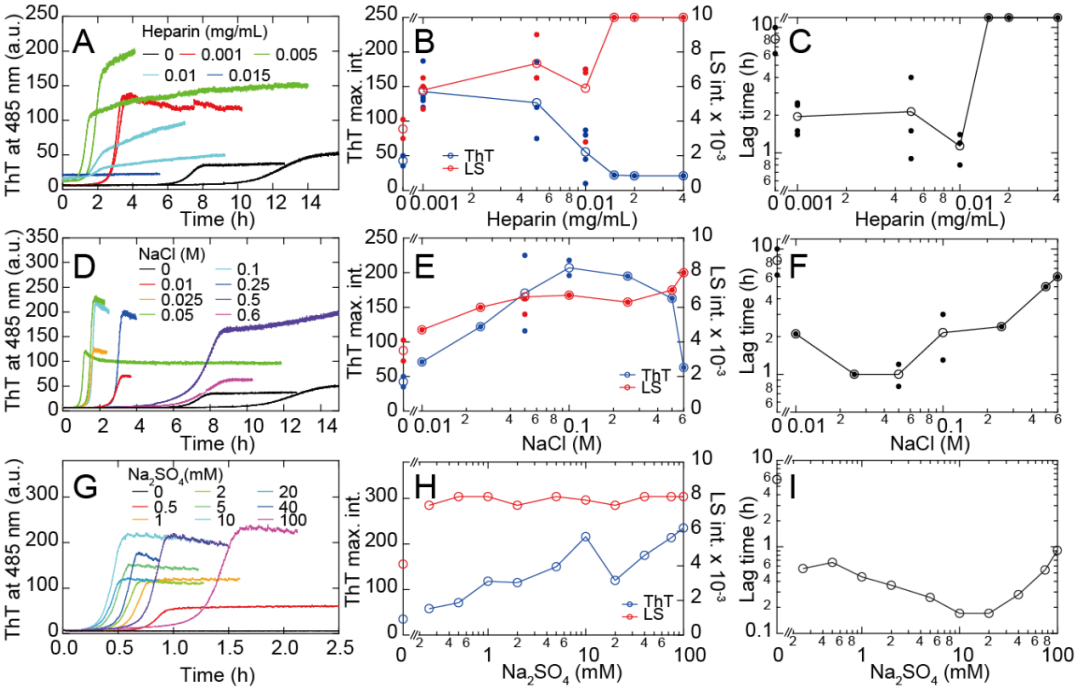

Fig. S10. Au nanoparticle-dependent fibrillation in 50% (v/v) TFE. (A-D) Kinetics of HEWL fibrillation in the presence of 0-50 nM AuNP monitored by ThT fluorescence (blue lines) and light scattering (red lines). (E) Schematic images of the interactions of HEWL with AuNP coated with sulfate groups. (F, G, H) AuNP concentration-dependence of lag time (F), maximum ThT fluorescence (G) and maximal light scattering (H). Original data points (small closed symbols) and their average values (open symbols) are shown. (I-L) Kinetics of HEWL fibrillation in the presence of 0-200 nM AuNP monitored by ThT fluorescence with HANABI. (M, N) Dependencies of the lag time (M) and maximal ThT fluorescence intensity (N) on AuNP concentration. Original data points (small closed symbols) and their average values (open symbols) are shown. (O, P) CD spectra before (O) and after ultrasonic treatment (P). (Q-T) EM images of fibrils obtained at 0 (Q), 5 (R), 10 (S), 50 (T) nM AuNPs with magnification of 20,000. (U) Image of fibrils at 50 nM AuNPs at a magnification of 50,000. Gold nanoparticles were found as black dots bound to fibrils.